Nanotechnology

PURPOSE-LED PUBLISHING™

PAPER • **OPEN ACCESS**

Fabrication and characterization of bioresorbable, electroactive and highly regular nanomodulated cell interfaces

To cite this article: Alice Lunghi *et al* 2025 *Nanotechnology* **36** 015301

View the article online for updates and enhancements.

You may also like

- Robust topological insulating property in C_2X-functionalized III-V monolayers
Xianghong Xue, Zhihua Lin, Rui Gao et al.
- Roadmap on printable electronic materials for next-generation sensors
Vincenzo Pecunia, Luisa Petti, Joseph B Andrews et al.
- Tuning the structure and properties of carbon cloth by $FeCl_3$ intercalation for efficient two-electron oxygen reduction catalysis
Yu Gao, Guangyuan Liang, Huanhuan Liang et al.

This content was downloaded from IP address 137.204.150.14 on 28/10/2024 at 13:09

OPEN ACCESS
IOP Publishing
Nanotechnology

Nanotechnology **36** (2025) 015301 (12pp) https://doi.org/10.1088/1361-6528/ad8096

Fabrication and characterization of bioresorbable, electroactive and highly regular nanomodulated cell interfaces

Alice Lunghi[1,2,3,*], Federica Velluto[1,2], Luana Di Lisa[4], Matteo Genitoni[1,2], Fabio Biscarini[1,5], Maria Letizia Focarete[4,6], Chiara Gualandi[4,7] and Michele Bianchi[5,*]

[1] Centre for Translational Neurophysiology of Speech and Communication, Istituto Italiano di Tecnologia, 44121 Ferrara, Italy
[2] Section of Physiology, Università di Ferrara, 44121 Ferrara, Italy
[3] Department of Physics, Informatics and Mathematics, Università degli Studi di Modena e Reggio Emilia, 41125 Modena, Italy
[4] Department of Chemistry 'Giacomo Ciamician' and INSTM UdR of Bologna, Alma Mater Studiorum, Università di Bologna, 40126 Bologna, Italy
[5] Department of Life Sciences, Università degli Studi di Modena e Reggio Emilia, 41125 Modena, Italy
[6] Health Sciences & Technologies (HST) CIRI, University of Bologna, 40064 Ozzano Emilia, Italy
[7] Interdepartmental Centre for Industrial Research on Advanced Applications in Mechanical Engineering and Materials Technology, CIRI-MAM, University of Bologna, 40136 Bologna, Italy

E-mail: alicelunghi@unimore.it and michele.bianchi@unimore.it

Received 27 March 2024, revised 28 August 2024
Accepted for publication 27 September 2024
Published 14 October 2024

Abstract

Biomaterial-based implantable scaffolds capable of promoting physical and functional reconnection of injured spinal cord and nerves represent the latest frontier in neural tissue engineering. Here, we report the fabrication and characterization of self-standing, biocompatible and bioresorbable substrates endowed with both controlled nanotopography and electroactivity, intended for the design of transient implantable scaffolds for neural tissue engineering. In particular, we obtain conductive and nano-modulated poly(D,L-lactic acid) (PLA) and poly(lactic-*co*-glycolic acid) free-standing films by simply iterating a replica moulding process and coating the polymer with a thin layer of poly(3,4-ethylendioxythiophene) polystyrene sulfonate. The capability of the substrates to retain both surface patterning and electrical properties when exposed to a liquid environment has been evaluated by atomic force microscopy, electrochemical impedance spectroscopy and thermal characterizations. In particular, we show that PLA-based films maintain their surface nano-modulation for up to three weeks of exposure to a liquid environment, a time sufficient for promoting axonal anisotropic sprouting and growth during neuronal cell differentiation. In conclusion, the developed substrates represent a novel and easily-tunable platform to design bioresorbable implantable devices featuring both topographic and electrical cues.

* Authors to whom any correspondence should be addressed.

Original content from this work may be used under the terms of the Creative Commons Attribution 4.0 licence. Any further distribution of this work must maintain attribution to the author(s) and the title of the work, journal citation and DOI.

© 2024 The Author(s). Published by IOP Publishing Ltd

Supplementary material for this article is available online

Keywords: surface nanomodulation, bioresorbable interfaces, neural tissue engineering, PEDOT:PSS, poly(lactic acid), poly(lactic-*co*-glycolic acid)

1. Introduction

With an estimated annual global incidence from 40 to 80 cases per million population, spinal cord injuries (SCI) impact the quality of life of a massive number of people, causing partial or total loss of motor and sensory function, also shortening patients' life expectancy [1, 2]. Lesions of the spinal cord (SC) most commonly depend on traumatic episodes likewise car accident and falls. Unfortunately, the clinical scenario lacks effective solutions to treat SCI: currently available options are limited to pharmacological and non-pharmacological treatment that do not offer a complete recover, but rather slow down the progress of the symptoms [3]. Thanks to recent breakthrough advances in neurosciences, brain–spine interfaces generated great hope about the functional restoration of the injured SC [4]; in particular the group lead by G. Courtine reported the successful rehabilitation of a tetraplegic patient that was able to walk naturally thanks to a digital brain–spine bridge [5]. The social impact and clinical relevance of this therapeutic approach are undeniably tremendous; however, the recovery of motor function is contingent on the proper functioning of the digital apparatus, still making the patient dependent on a prothesis. Re-establishing the physical connection of the interrupted SC represents the definitive way to tackle SCI as it would allow to restore the physiological transmission of neural signals and, consequently, of the motor and/or sensory function [3, 6, 7]. To this end, autologous transplant of stem cells has emerged as a very promising strategy to support axonal reconnection [6–8], especially by reducing the formation of a non-permissive environment that hinders cell development. Nonetheless, simple cell stem transplant lacks two essential elements: a spatially delimited environment capable to prevent spontaneous migration of the cells and one or multiple stimuli to induce cell differentiation toward the desired phenotype [6, 7, 9]. In this scenario, implantable 3D scaffolds have been extensively studied as they offer a platform that simultaneously constrains transplanted cells to the site of the lesion and allows to deliver different signals to guide cells commitment (release of small molecules and growth factors, topographical guidance, electrical stimulation, etc) [9–13]. Implantable scaffolds for neural tissue engineering aim to support nerve and SC regeneration by guiding axonal reconnection. Owing to the longitudinal organization of the nervous system, scaffolds that physically bridge the lesion (conduits) supply neurons with pre-determined growth path, establishing a preferred direction for neurites elongation [14–17]. Moreover, hierarchical organization of such scaffolds (e.g. hydrogel embedding, internal frameworks, multichannel structure, etc) further support nerves regeneration by integrating multiple levels of guidance and stimulation [12–14, 18, 19]. In particular, the presence of surface micro- and nanostructures likewise pillars, cones, wires and grooves, demonstrated to greatly enhance neurites outgrow and synapsis formation [18, 20–23] by providing a spatially organized environment that mimics the architecture of the extracellular matrix and the organization of the glia [24]. Among all the different topographies, aligned nanogrooves were demonstrated to act as preferential tracks that neurites follow during the elongation process, further guiding the reconnection process [13]. Also, nanogrooves whose width is comparable to axons' diameter (typically 1 μm for mammal neurons) showed the best guiding capability compared to substrates with wider or narrower nanogrooves [13, 25–27]. Beside the typical longitudinal organization of the ECM, the nervous system is characterized by intrinsic electrical conductivity thus electrical stimulation represent an elegant strategy to further promote axonal reconnection [13, 19, 23, 28]. *In vitro* application of mild electric field demonstrated to foster neurites sprouting and boost their elongation [13, 29, 30]. Due to their electroactive properties and organic nature, (semi)conductive polymers (CPs) gained a prominent role in this research field [18, 19, 23, 25, 31], with particular outstanding performances of poly(3,4-ethylendioxythiophene) polystyrene sulfonate (PEDOT:PSS). PEDOT:PSS owes its success to high biocompatibility, water processability, flexibility, high electrical capacitance and low impedance [32–34], that allows to stimulate cells by applying low voltage trains [13, 29]. We recently reported the successful integration of regular topographical guidance and electrical stimulation demonstrating their synergic cooperation in enhancing oriented axonal development *in vitro* [13]. Keeping in mind that the ultimate goal would be to develop a device capable to sustain SC regeneration *in vivo*, we attempted to translate both the topographical guidance and the electrical conductivity to an implantable and bioresorbable substrate. Bioresorbable materials are highly desired in clinical practice as they eliminate the need of surgical removal [7, 9, 17, 35]. However, even though bioresorbable scaffolds capable to actively promote SC regeneration would represent the novel frontier of neural tissue engineering and the undeniable benefits represented by topographic and electric cues in promoting axonal reconnection, very little has been done to combine topographical guidance, electrical stimulation and bioresorbability in a single device, although literature offers several examples of scaffolds combining two out of these three characteristics [36]. Nonetheless, most of them are obtained starting from conductive blends extruded

into partially aligned nanofibers by means of electrospinning [37], hence offering only a limited control over the topographical organization [38, 39]. Some groups explored the possibility to overcome this limitation and to obtain regular surface patterns by means of (soft)lithography and to combine geometrical cues either with bioresorbability or electroactivity [40–42]. Since we demonstrated [13] that high regularity of the anisotropic surface pattern is crucial to promote axonal alignment and elongation and that the process is accelerated when paired with electrical stimulation, here we explored the possibility to implement nanogrooved topography and electrical conductivity on biodegradable and bioresorbable films, being the first step towards the translation of this strategy to regenerative medicine applications. We opted for two polyesters, namely poly(D,L-lactic acid) (PLA) and poly(lactic-*co*-glycolic acid) (PLGA), as substrate material and we designed an *ad hoc* fabrication route to integrate surface nanomodulation and electrical properties on free-standing PLA and PLGA films. PLA and PLGA are approved by the FDA for human use and have been used in medical practice for almost 30 years, with application in several different fields (ophthalmological surgery [43], bone prothesis [44], vascular tissue engineering [45], etc). To date, PLA-based scaffolds for neural tissue engineering are limited to *in vitro* testing, with few examples of successful animal trials [46], whereas PLGA implants have reached clinical human trials [47]. Here, we report fabrication, morphological and electrical characterization of the nanomodulated and conductive polyester films (nanoPEDOT/-PLA and nanoPEDOT/PLGA), also demonstrating the capability of such substrates to maintain their features over a period of time compatible with neurites development and maturation.

2. Methods and materials

Fabrication of nanomodulated polymer based PEDOT:PSS substrates. Free-standing (PLA, Resomer® R 207 S, Evonik, CA, USA. Inherent viscosity = 1.3–1.7 dL g^{-1}, MW = 118 000 g mol^{-1}, PDI = 1.8) and (PLGA, Sigma Aldrich, MO, USA. Lactide:glycolide molar ratio = 75:25, MW = 66 000–107 000 g mol^{-1}) thin films were obtained by replica molding of a polydimethylsiloxane (PDMS) stamp. A commercial polycarbonate (PC) compact disc (CD; pitch 1.5 μm, groove width ∼650 nm; ridge width ∼850 nm; ridge height ∼180 nm) was employed as a sacrificial substrate to obtain nanomodulated and unmodulated (flat) PDMS mold using the front and the rear part of the CD, respectively. To obtain the nanomodulated mold, the CD protective layer was peeled off to expose the patterned surface and the antistatic layer was removed by abundant rinsing in ethanol followed by 15 min of sonication (1:1 v/v ethanol:MilliQ water); then the PC sacrificial substrate was dried under nitrogen flow. The PDMS mold was fabricated using the Sylgard 184 Elastomer Kit (Dow Europe GmbH, Horgen, Switzerland) by mixing the silicon elastomer base and the elastomer base curing agent in a 10:1 v/v ratio. The mixture was allowed to spontaneously degas for 1 h, poured onto the PC sacrificial substrate (nanomodulated face up) and cured overnight at 60 °C, then the sacrificial PC substrate was removed from the stamp. Solutions of PLGA and PLA were prepared by dissolving either PLGA or PLA in tetrahydrofuran (THF, anhydrous, purity ⩾ 99%, Sigma Aldrich, MO, USA) to obtain a final concentration of 10% w/v. 1 ml of polyester (either PLA or PLGA) solution was drop-casted on the PDMS mold and the solvent was allowed to evaporate overnight at room temperature. Before peeling the stamp off, the polyester film was cured for 2 h at 60 °C to remove any eventual residue of the solvent. Nanomodulated substrates (nanoPLA; nanoPLGA) were coated with a thin film of PEDOT:PSS by electrodeposition. Prior to electrodeposition, substrates surface was metallized by depositing a sheer gold layer of ∼30 nm (nanoAu/-PLA; nanoAu/PLGA). Metallization was obtained by mean of DC magnetron plasma sputtering (Quorum Tech, London, UK) using a 99.99% pure gold target and working in Argon rarefied atmosphere (pressure $\sim 10^{-3}$ mbar; average current ∼18 mA, 120 s). PEDOT:PSS was electrodeposited on the metalized surface of the polyester films via chronocoulometry. Electrodeposition was carried out in a three-electrode electrochemical cell filled with a solution of 0.01 M ethylenedioxytiophene (EDOT; Sigma Aldrich, MO, USA) and 0.8% w/w sodium polystyrene sulfonate (NaPSS, Sigma Aldrich, MO, USA) using a standard AgIAgCl (3 M KCl) as reference electrode (RE), a large area platinum mesh (15 × 15 mm^2) as counter electrode (CE) and nanoAu/PLA or nanoAu/PLGA film as working electrode (WE). The potentiostat (Gamry Reference 600, Gamry Instruments, PA, USA) was set to supply a constant potential of 1 V to the WE and the amount of the deposited charge was limited to 50 mC cm^{-2}, resulting in a reproducible thickness of the PEDOT:PSS coating. Unmodulated films (flatPLA; flatPLGA) were fabricated with the same procedure using a PDMS mold obtained by exposing the unmodulated side of the PC sacrificial substrate to the PDMS.

Electrochemical characterization. Electrochemical properties of metallized and PEDOT:PSS-coated substrates, either nanomodulated or flat, were evaluated by electrochemical impedance spectroscopy (EIS). EIS was measured in the frequency range 1–10^5 Hz using a Gamry Reference Potentiostat 600 (Gamry Instrument, PA, USA). EIS measurements were carried out in physiological saline solution (NaCl 0.15 M) in a three-electrodes electrochemical cell, using a standard AgIAgCl (3 M KCl) as RE and a large area platinum mesh (15 × 15 mm^2) as CE. Metalized and PEDOT:PSS-coated polyester films were set as WE.

Electrical characterization. In-plane sheet resistance (R_S) of both flat and nanomodulated PEDOT:PSS-coated substrates was extracted from four-point probe measurements. A square area of 1 × 1 cm^2 was delimited on the sample surface and four blunt stainless-steel probes were placed in contact with the vertices. Using a two-channel source measure unit (Keysight, CA, USA) a constant value of current (0.1 mA) was forced

for 10 s; then the current was raised to 0.5 mA with steps of 0.1 mA each. Four-point probe experiments were conducted in dry (in air, room temperature) and hydrated conditions, the latter obtained by soaking the sample in a phosphate buffer saline (PBS) solution overnight at room temperature. Resistance (R) was extracted from Ohm's law and used to calculate the R_S according to the following equation [48]:

$$R_S = \frac{R \times \pi}{\ln 2}.$$

Atomic force microscopy (AFM) analysis. Surface topography of the bare, gold sputtered and PEDOT:PSS-coated nanomodulated PLA and PLGA films was investigated by AFM using a Park XE7 AFM system (Park System, Suwon, Republic of Korea). Images were acquired in tapping mode operating in air and at room temperature. Silicon cantilever with Al reflective backside coating, typical curvature radius ∼7 nm, elastic constant ∼26 N m^{-1} and resonance frequency ∼300 kHz were used (OMCL-AC160TS, Olympus Micro Cantilever, Tokyo, Japan). Typical dimensions of the pattern's features and root-mean-square surface roughness (RMS) were analysed by the Park System XEI software (Park System, Suwon, Republic of Korea).

Water contact angle measurements. Water contact angle was evaluated by using a home-build contact angle measurement unit. For each group of substrates (bare and PEDOT:PSS-coated PLA and PLGA films, both flat and nanomodulated) images were collected and analysed with ImageJ freeware (Rasband, W.S., ImageJ, U.S. National Institute of Healt, Bethesda, Maryland, USA; https://imagej.nih.gov/ij/, 1997–2018) [49]. Water contact angle values were averaged over at least four samples for each group.

Maintenance of surface topography. The capability of PEDOT:PSS-coated nanomodulated films (nanoPEDOT/-PLA; nanoPEDOT/PLGA) to preserve their morphological characteristics upon prolonged exposure to a liquid environment was tested by soaking the samples in PBS (1X, pH 7.4; Sigma Aldrich, MO, USA) at 37 °C up to 3 weeks. Maintenance of the original surface topography was investigated with AFM as described above after 1, 2 and 3 weeks of immersion in PBS.

Thermogravimetric analysis (TGA) and differential scanning calorimetry (DSC). TGA were carried out using a TGA Q500 TGA (TA Instruments, DE, USA). The thermograms were recorded from room temperature to 700 °C, at a heating rate of 10 °C min^{-1}, under nitrogen flow. DSC measurements were carried out under nitrogen flow by mean of a differential scanning calorimeter (DSC Q100; TA Instruments, DE, USA) equipped with a Refrigerated Cooling System (RCS 90). Samples were subjected to two heating scans at 20 °C min^{-1} in the temperature range −90 °C–250 °C and one fast cooling, applied between the heating scans.

Data analysis and statistics. Data were analysed with OriginPro 2020 software (OriginLab Corporation, MA, USA) and reported as mean ± standard deviation. Significance threshold was set at $p < 0.05$.

3. Results and discussion

NanoPEDOT/PLA and nanoPEDOT/PLGA substrates. Free-standing, nanomodulated and conductive PLA and PLGA films were fabricated according to the procedure outlined in figure 1(a). The whole process was designed to transfer the submicron nanogrooved pattern of a sacrificial PC template onto PLA and PLGA surface with the highest fidelity. PC surface is impressed with an alternation of grooves and ridges with a pitch of ∼1.5 μm and a duty ratio (defined as the ratio between the groove width and the total pitch) of 43% (figure 1(b)); in a recently published work [13] we demonstrated that this pattern is capable to greatly influence neurites alignments as the width of the nanogrooves well suits the typical diameter of mammal neurites (∼1 μm) [27, 50].

As such, high-fidelity replica of the original pattern on nanoPLA and nanoPLGA films is essential to provide optimal topographical guidance to the elongating neurites. For this reason, we first obtained the negative image of the PC pattern on a PDMS mold that was then employed to transfer the original PC pattern on PLA and PLGA free-standing films. NanoPLA and nanoPLGA were made conductive by coating their surface with a thin film of PEDOT:PSS. To avoid the concealing of the underlying topography, we electrodeposited PEDOT:PSS via chronocoulometry, a technique that allows for a fine control of the amount of the deposited charge, that was limited to 50 mC cm^{-2}, thus providing precise control of PEDOT:PSS thickness (∼50 nm). An intermediate sheer layer of gold was sputtered on nanoPLA and nanoPLGA surface to prepare the substrates for the electrodeposition process (nanoAu/PLA; nanoAu/PLGA). Upon deposition of the gold thin layer, an increase in grooves width (and a consequent reduction in ridges width) for both nanoAu/polyester substrates was observed (figures 2(a) and (b)). Indeed, original groove width in nano/PLA and in nano/PLGA was 0.54 μm and 0.55 μm, respectively, and it was increased up to 0.63 (nanoAu/PLA) and 0.64 μm (nanoAu/PLGA) (table S1). This behaviour can be explained considering the mild vacuum condition of the metallization process that causes the elimination of micro-sized air bubbles trapped in the films, resulting in a slight change of features dimensions. The deposition of the PEDOT:PSS film caused a narrowing of the grooves, whose width was reduced to 0.56 μm in nanoPEDOT/PLA and to 0.55 μm in nanoPEDOT/PLGA. As expected, an opposite behaviour was observed for the ridges whose width increased from 0.72 μm (nanoAu/PLA) to 0.84 μm for nanoPEDOT/PLA and from 0.74 μm (nanoAu/PLGA) to 0.87 μm for nanoPEDOT/PLGA. The opposite behaviour of grooves and ridges (i.e. narrowing vs. thickening) indicates that PEDOT:PSS electrodeposition occurs on the entire surface of the substrate, including on grooves' lateral walls, suggesting an uniform coating of the pattern. Groove height

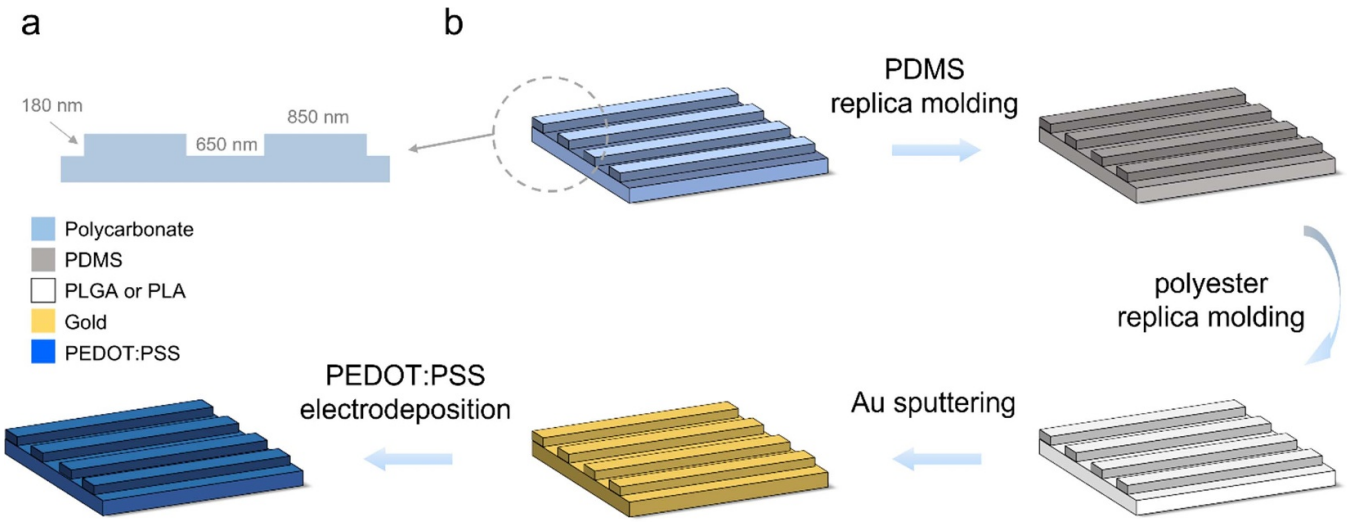

Figure 1. Fabrication of nanoPEDOT/PLA and nanoPEDOT/PLGA. (a) Characteristic dimensions of pattern features (in scale). (b) Schematic of the fabrication process. The polycarbonate sacrificial substrate (i) is replicated through replica molding to obtain the PDMS stamp (ii) that is further replicated to obtain either nanoPLA or nanoPLGA (iii). NanoAu/PLA and nanoAu/PLGA (iv) are obtained by mean of gold sputtering; then PEDOT:PSS is electrodeposited on substrates metalized surface, yielding either nanoPEDOT/PLA or nanoPEDOT/PLGA (v).

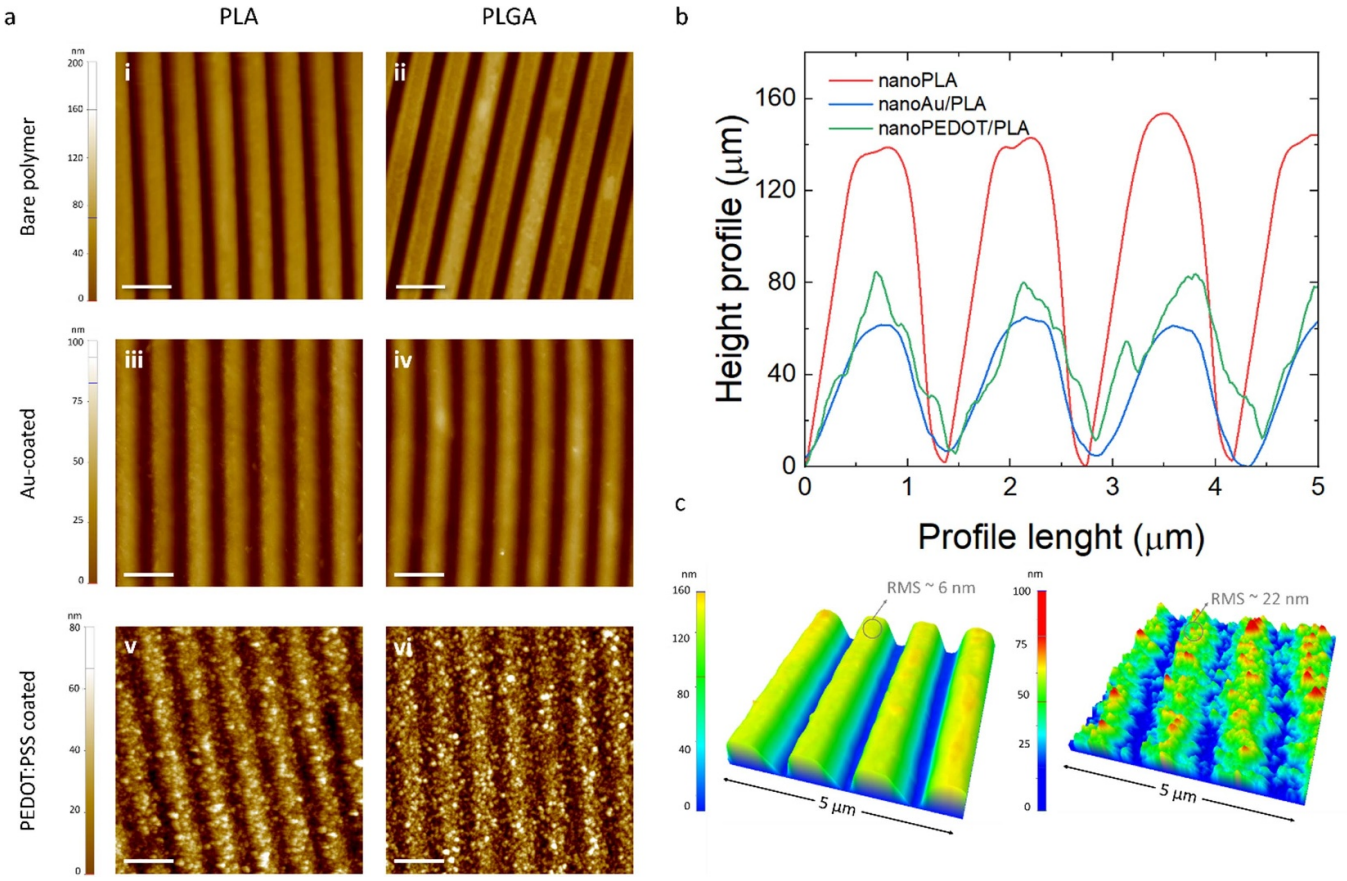

Figure 2. AFM analysis of nanoPEDOT/PLA and nanoPEDOT/PLGA surface topography. (a) 2D topography images of bare (i), (ii); Au coated (iii),(iv) and PEDOT:PSS coated (v), (vi) nanomodulated PLA (i), (iii), (v) and PLGA (ii), (iv), (vi) films. (b) Height profile of nanoPLA, nanoAu/PLA and nanoPEDOT/PLA. (c) 3D rendering of nanoPLA (i) and nanoPEDOT/PLA (ii) showing local surface RMS. Height profiles and 3D renderings of PLGA-based samples are reported in figure S1.

was the most variable parameter. Changes in its values upon metallization indicate that gold accumulates at the bottom of the grooves rather than at the top of the ridges and that also the PEDOT:PSS film grows faster between the grooves than on top of the ridges. Finally, it is worth noticing that groove and ridge width for both nanoPEDOT/PLA and nanoPEDOT/PLGA show no significant differences with the original PC sacrificial substrate (p-value > 0.05), meaning that the optimization of the fabrication procedure effectively preserves the surface pattern and avoids the distortion of the topography (figures 2(b) and S1).

Surface roughness is recognized to greatly influences the capability of a substrate to promote cell adhesion [51–53]; in particular, adhesion of neural cells has been reported to be adversely affected by extremely smooth (RMS < 10 nm) or rough (RMS > 70 nm) surfaces, while RMS values in the range 20–50 nm demonstrated to favour the adhesion process [54]. A considerable change in local surface RMS roughness (1×1 μm^2) between bare nanoPLA and nanoPLGA and their PEDOT:PSS-coated counterparts could be observed (figures 2(c) and (S1)). RMS of bare nanoPLA and bare nanoPLGA increased from ∼6 nm and ∼4 nm, respectively, to ∼21.5 nm (nanoPEDOT/PLA) and ∼19 nm (nanoPEDOT/PLGA), owing this increase the to the typical granular conformation of the electrodeposited polymer [55, 56] (p-value < 0.05 comparing RMS of bare nanomodulated polymers with their PEDOT:PSS coated counterparts). Notably, RMS values of nanoPEDOT/polyester substrates are in good agreement with optimal roughness range for cell adhesion [54]. Another important parameter capable to favour or not cell adhesion is surface wettability [22, 57, 58]. As expected, nanoPEDOT/PLA and nanoPEDOT/PLGA resulted significantly (p-value < 0.05) more hydrophilic than their bare nanomodulated counterparts. Water contact angle (figure S2) decreases from ∼88° for both nanoPLA and nanoPLGA to ∼31° for nanoPEDOT/PLA and ∼34° for nanoPEDOT/PLGA. The more electrostatic nature of PEDOT:PSS compared to PLA and PLGA promotes the adhesion and spreading of water molecules on the surface, thus increasing the wettability of the substrates. While bare nanomodulated films, either nanoPLGA and nanoPLA, are significantly more hydrophobic (p-value < 0.05) than their flat counterparts, the difference between the wettability of nanoPEDOT/polyester and flatPEDOT/polyester is negligible (p-value > 0.05). This behaviour can be ascribed to the effect of the pattern: nanotoporaphy influences the wettability of the bare polymers, but its effect is overshadowed by the presence of the PEDOT:PSS layer; suggesting that in this case the chemical nature of the surface contributes more to the wettability than the topography.

Electrochemical and electrical characterization of the substrates. One of the most appealing characteristics of PEDOT:PSS is its low impedance. In general, whenever a metallic electrode is coated with PEDOT:PSS, the impedance of the electrode decreases [59], making PEDOT:PSS coatings suitable for a wide plethora of biological applications. Substrates exhibiting low impedance (Z) and stable sheet resistance (R_S) in dry and wet conditions allow to stimulate neural cells with low-voltage potential trains [13]; hence, in the view of integrating topographical guidance and electrical stimulation on biocompatible and bioresorbable substrates, these two features are highly desirable. Impedance of metallized and PEDOT:PSS-coated substrates, both nanomodulated or flat, was evaluated by mean of EIS over a broad frequency range (1–10^5 Hz).

As shown in the Bode plot reported in figure 3(a), in the low frequency domain (1–100 Hz) nanoPEDOT/PLA and nanoPEDOT/PLGA show $|Z|$ values up to one order of magnitude lower than their metalized counterpart: at 1 Hz, the addition of the PEDOT:PSS layer causes the impedance to drop from ∼400 Ω (gold metallized) to ∼20 Ω (PEDOT:PSS-coated). This behaviour indicates an optimal coupling between the metallic layer and the CP, allowing for a good charge transport between the underlying Au layer and the PEDOT:PSS film. In the high frequency region, instead, a similar $|Z|$ values for nanoAu/polyester and nanoPEDOT/polyester can be noticed, suggesting that the resistive behaviour of PEDOT:PSS is overshadowed by the resistance of the gold film. Finally, nanoPEDOT/PLA and nanoPEDOT/PLGA show a similar change in the cut-off frequency that shifts from ∼10^2 Hz (nanoAu/polyester) to less than 10 Hz. These results indicate that, as expected, the overall electrochemical behaviour of the nanomodulated films is not influenced by the chemical nature of the polyester (either PLA or PLGA), but solely depends on the PEDOT:PSS coating. Similar considerations can be done for flat substrates (figure S3): compared to their metalized counterparts, in the low frequency domain flatPEDOT/polyester films exhibit lower $|Z|$ values, with one-order-of-magnitude drop at 1 Hz; while in the high frequency region, $|Z|$ values of metallized and PEDOT:PSS-coated substrates are similar. As for the nanomodulated substrates, the cut-off frequency is shifted from ∼10^2 Hz (flatAu/polyester) to values lower than 10 Hz (flatPEDOT/polymers). It is worth noticing that $|Z|$ at 1 Hz is slightly higher for flatPEDOT/polyester substrates (∼35 Ω) than for nanoPEDOT/polyester films (∼20 Ω) as shown in figure 3(b). This difference can be ascribed to the higher surface area of the nanomodulated substrates, being the latter contributed also by the area of grooves' lateral walls. Electrical properties of the PEDOT-coated substrates, both flat and nanomodulated, were assessed by mean of four-point probe measurements. In-plane sheet resistance of the substrates was measured both in dry (in air at room temperature) and in wet condition (overnight immersion in PBS at room temperature) to evaluate how ions intake influences the electrical properties of the substrates. Envisioning future clinical applications of the substrates, it is essential that the PEDOT:PSS-coated films retain low in-plane R_S when exposed to an environment that mimics the pH and the ionic strength of physiological conditions as electrical stability of these substrates is fundamental to guarantee reliable stimulation protocols *in vivo*. R_S values of NanoPEDOT/PLA and nanoPEDOT/PLGA and their flat counterparts (figure 3(c)) are in good agreement with those reported in literature [60, 61]. As a consequence of ions intake, wet R_S values were higher than in dry condition; however, no significant differences were found between R_S values of flatPEDOT/PLA and nanoPEDOT/PLA

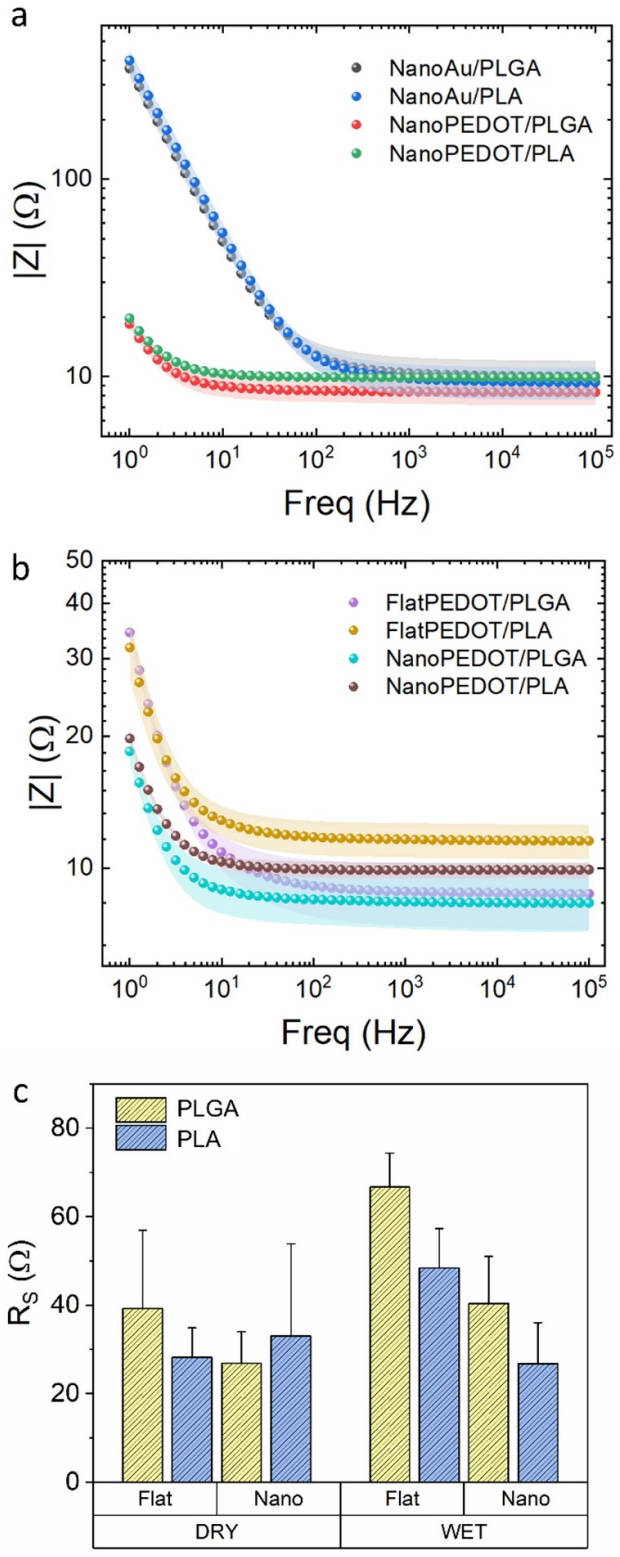

Figure 3. Electrochemical and electrical characterization of nanoPEDOT/PLA and nanoPEDOT/PLGA. (a) EIS spectra of the metalized and PEDOT-coated nanomodulated samples. (b) EIS spectra of the PEDOT-coated flat and nanomodulated films. (c) Sheet resistance of flat and nanomodulated PEDOT-coated samples under dry and wet conditions.

and between flatPEDOT/PLGA and nanoPEDOT/PLGA (p-value > 0.05) either in dry or wet conditions, suggesting that the presence of the nanotopography do not affect in-plane R_S of the PEDOT:PSS-coated films. Finally, no statistical difference (p-value > 0.05) could be appreciated between PLGA and PLA substrates, confirming that the different chemical nature of the polyester plays no role in defining electrical properties of the substrates.

Polymer degradation and maintenance of surface topography. One of the most important features of bioresorbable implants is their ability to degrade at a rate comparable to that of tissue regeneration. When implanted *in vivo*, PLA and PLGA show complete degradation and total loss of mass over 24–30 months [62]. The *in vivo* degradation process of polyhydroxyacids involves the hydrolytic cleavage of esters bonds with a consequent reduction of chain length and, at longer times, with the progressive dissolution of water-soluble short molecules. The consequent reduction of polymer molecular weight may lead to significant change in the material characteristics, well before its complete degradation, such as change in thermal and mechanical properties and in water uptake. As the topography of nanoPEDOT/polyester is intended to direct the elongation of neurites, the ability of the substrates to retain the surface nanomodulation over a period sufficient for cells to develop their protrusion is indispensable. As such, we evaluated the capability of nanoPEDOT/PLA and nanoPEDOT/PLGA to provide a reliable guidance when exposed to an environment that favours PLA and PLGA degradation by assessing changes in the width and depth of the grooves after soaking the samples in PBS (pH 7.4) at 37 °C up to 3 weeks. We opted to limit the timeframe of the degradation experiments to three weeks since we previously demonstrated that on the same pattern with the same surface texture neurites alignment can be appreciated already after six days [13].

As shown in figure 4(a-i), groove width of nanoPEDOT/PLA remained almost unchanged over the 3 weeks; for nanoPEDOT/PLGA, on the contrary, the narrowing of the grooves was evident already after 1 week, with an overall reduction of ∼215 nm (p-value < 0.05) after 3 weeks of immersion in PBS. A corresponding behaviour could be observed for the ridges (figure 4(a-ii)): similar width values with no significant differences over the 3 weeks were found for nanoPEDOT/PLA samples, while for nanoPEDOT/PLGA the widening of the ridges was found to be significant (p-value < 0.05) already after 1 week. With respect to the height of the pattern features, PLA and PLGA showed opposite trends (figure 4(a-iii)); indeed, groove height of nanoPEDOT/PLGA consistently decreased from ∼55 nm in the pristine samples (i.e. not soaked in PBS) to ∼30 nm after 3 weeks of soaking in PBS, while groove height of nanoPEDOT/PLA increased from ∼55 nm in the pristine samples to ∼75 nm (p-value < 0.05 in both cases). Overall, nanoPEDOT/PLA shows a superior capability to maintain surface nanomodulation than nanoPEDOT/PLGA.

Differences in the behaviour of the two polyesters can be explained advocating the more hydrophilic nature of PLGA

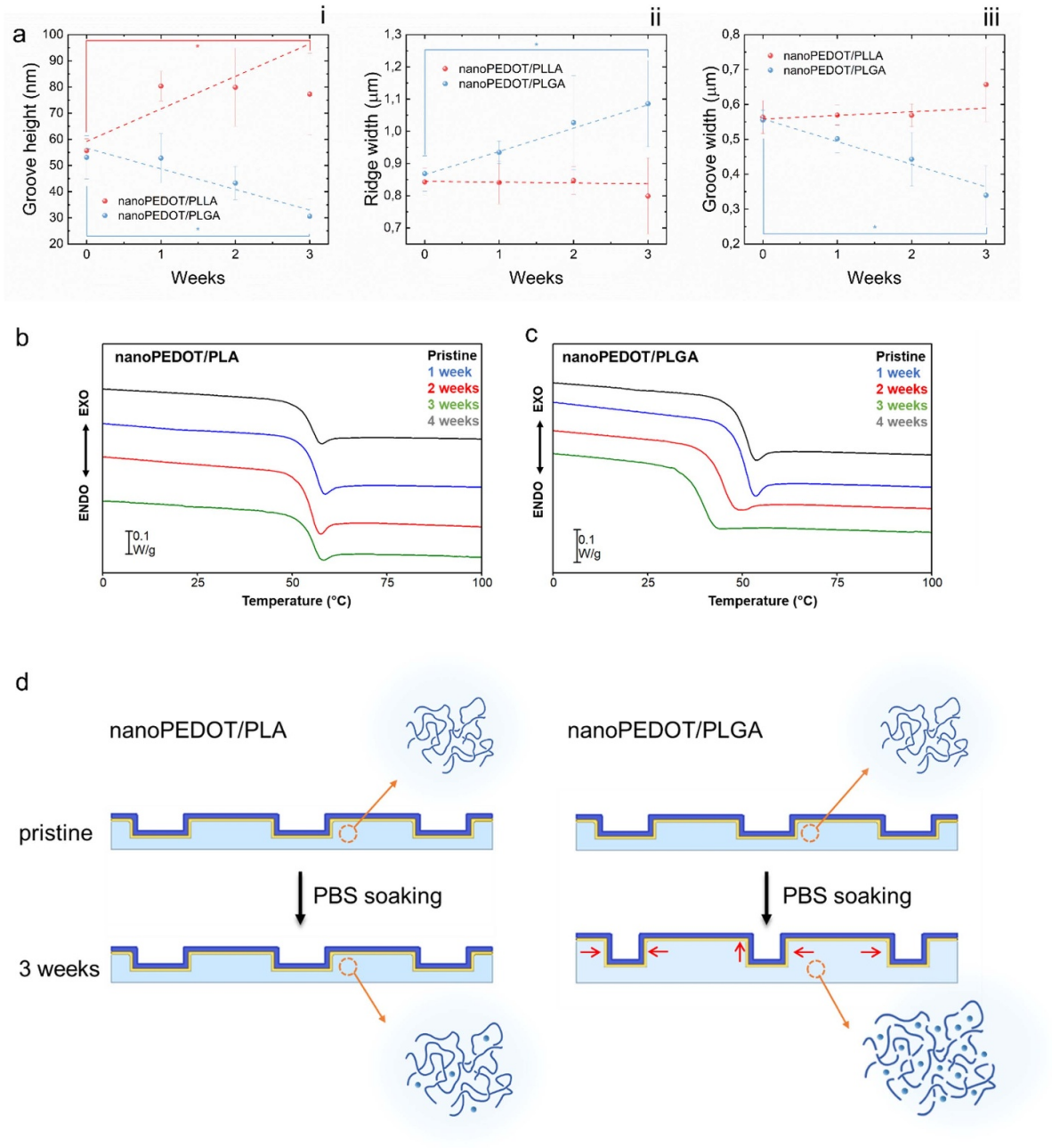

Figure 4. Maintenance of surface nanomodulation. (a) Variation of groove width (i), ridge width (ii) and groove height (iii) of nanoPEDOT/PLA (red) and nanoPEDOT/PLGA (blue) upon soaking in PBS at 37 °C up to 3 weeks; dashed lines are a guide-for-the-eye (*p-value < 0.05). DSC second heating scan after fast cooling of (b) nanoPEDOT/PLA and (c) nanoPEDOT/PLGA. (d) Schematic representation of the proposed mechanism for topography deformation. Red arrows in the bottom right model are a guide-for-the-eye to show the direction of topography deformation (from the left: nanogrooves narrowing, height increase and nanoridges widening).

compared to PLA. As extensively reported in the literature, higher content of hydrophilic glycolic acid units in the copolymers facilitated the absorption and diffusion of water [63–65]. This determines a different hydrolytic degradation kinetics, with PLGA copolymers degrading faster than PLA [63–65]. When immersed in an aqueous environment for 3 weeks, both nanoPEDOT/PLA and nanoPEDOT/PLGA does not show a significant change of weight (figure S4). This result is in line with previous studies that demonstrated that, for these kinds of polymers, the weight remains constant in the first weeks of the degradation and that weight loss is recorded at longer times, namely when the molecular weight had decreased below a critical value and soluble oligomers formed. Change of polymer molecular weight during degradation is typically monitored by Gel Permeation Chromatography which, however, is unfeasible in our specific case, since the polymers are coated with PEDOT:PSS and gold.

To shed light on the structural stability of the substrates over prolonged exposure to an aqueous environment, we characterized the behaviour of nanoPEDOT/PLLA and nanoPEDOT/PLGA using TGA and DSC. In the TGA analysis (figure S5), both pristine samples show a weight loss at the temperature of 100 °C of ca. 6 wt.%, ascribable to residual solvent after film casting. This weight loss is no longer detectable in the samples exposed to water, which is expected since water exposure is known to effectively removes residual THF due to the solvent's polarity and high miscibility in water. All samples exhibited a weight loss attributed to the thermal degradation of the PLA and PLGA components. As the duration of exposure to the buffer increased, the thermal degradation of both samples shifted to lower temperatures (T_{max} in table S2), indicating a notable decrease in thermal stability. This observation can be rationalized by the reduction in polymer molecular weight resulting from hydrolytic degradation. It aligns well with previous findings demonstrating the dependence of polyester thermal stability on molecular weight, wherein a decrease in molecular weight corresponds to shorter polymer chains [66]. These results confirm that both polymers underwent hydrolysis during the 3 week degradation period, despite no gravimetric weight loss being recorded. DSC analysis (figures 4(b), (c) and table S2) indicates that the glass transition temperature (T_g) of PLA remained unaffected by immersion in PBS, being stable at 54 °C. Differently, after 3 weeks, the T_g of PLGA decreased by 11 °C compared to the pristine material, going from an initial value of 50 °C and reaching the value of 39 °C. This reduction in PLGA T_g further supports the decrease in polymer molecular weight, which is more pronounced compared to PLA, in line with the distinct hydrophilicity of the two polymers.

Hence, the poorer capability of PLGA to maintain the surface nanomodulation compared to PLA can be the consequence of a more extended hydrolysis in the former, where water molecules better penetrate the PLGA film from the uncoated side and intercalate between the chains, causing the ridges to swell and the grooves to narrow, ultimately resulting in a more evident deformation of nanoPEDOT/PLGA surface topography. The effect of water penetration and polymer swelling on the geometry of a PLGA patterned surface has been previously reported and modelled by some of us [67]. A schematic representation of the proposed mechanism is shown in figure 4(d). Overall, nanoPEDOT/PLA showed a better capability to maintain the surface nanomodulation than nanoPEDOT/PLGA, showing negligible changes in the original feature dimensions. Nonetheless, after 3 weeks of immersion in PBS at 37 °C, in both substrates it was still possible to recognize the nanopattern.

Another important aspect to consider is the surface microstructure (the roughness) as the effect of the topographical guidance would be of no utility if cells cannot reside on the substrate because of an environment that discourages cell adhesion. The feasibility of the substrates to provide cells with a long-term favourable environment was quantitatively investigated by evaluating changes in RMS values upon immersion in PBS. Over the 3 weeks, only little fluctuations of the RMS values were observed (25 ÷ 27 nm) both for nanoPEDOT/PLA and for nanoPEDOT/PLGA. Remarkably, RMS refers to the PEDOT:PSS coating suggesting that the prolonged exposure to an aqueous environment does not affect the CP, further supporting the hypothesis that water swelling occurs from the uncoated side of the substrate. NanoPEDOT/PLA and nanoPEDOT/PLGA are designed to simultaneously provide neural cells with topographical guidance and electrical stimulation, thus another essential characteristic of nanoPEDOT/-polyester films is to show stable electrochemical properties when exposed to an aqueous environment. After 3 weeks, EIS spectra of nanoPEDOT/PLA and nanoPEDOT/PLGA were in good agreement with those of the corresponding pristine substrate (figure S6). Notably, in both cases the cut-off frequency remained constant, suggesting that the charge transport between the PEDOT:PSS coating and the underlying Au layer is not affected by the immersion in PBS; also confirming that water molecules penetrate the substrates from the bare polyester side. Moreover, substrate conductivity is not affected by the little changes in the surface topography as, if it would, a bold increase in the entire frequency spectrum and an evident shift in the cut-off frequency would have been observed. Overall, electrochemical and morphological stability shown by nanoPEDOT/PLA and nanoPEDOT/PLGA upon 3 weeks of exposure to a liquid environment that mimics ionic strength, pH and temperature of the physiological one, points to the ability of such substrates to guarantee a reliable platform to sustain neuritogenesis and, eventually, promote axonal reconnection.

4. Conclusions

In this study, we successfully demonstrated the integration of electrical properties and surface nanomodulation on biodegradable and biocompatible free-standing substrates, being this a first step toward the design of implantable scaffolds for neural tissue engineering. Remarkably, we previously demonstrated that the synergic combination of topographical and electrical cues actively promotes neurites sprouting and elongation, also favouring alignment and axonal reconnection. The capability of nanoPEDOT/PLA and nanoPEDOT/PLGA to maintain surface nanomodulation and electrical properties upon prolonged exposure to a liquid environment makes them promising candidates for the *in vivo* application of such strategy. To do so, *in vitro* experiments aimed to probe biocompatibility and effectiveness of our nanomodulated, conductive and bioresorbable substrates in promoting neurites elongation and reconnection will be needed, together with long-time *in vivo* degradation test to explore the durability of the device and the effect of its degradation on the regeneration process. In conclusion, the results shown in this work pave the way for the design of advanced multifunctional implantable scaffolds for neural tissue engineering, opening to exciting perspectives in the field of regenerative medicine for SCI repair.

Data availability statement

The data cannot be made publicly available upon publication because no suitable repository exists for hosting data in this field of study. The data that support the findings of this study are available upon reasonable request from the authors.

Acknowledgments

The entire experimental work was carried out by A L and F V; L D L, M L F and C G contributed to TGA and differential scanning calorimetry. Data analysis was carried out by A L, F V and L D L with the contribution of M.G. The manuscript was written through the contribution of A L; M B; G C and F V and it was revised, read and approved by all the authors. The work was conceptualized and supervised by M B with the contribution of C G, M L F and F B.

The work has been founded by the National Recovery and Resilience Plan (NRRP), Mission 04 Component 2 Investment 1.5—NextGenerationEU, Call for tender n. 3277 dated 30/12/2021, Award Number: 0001052 dated 23/06/2022.

Conflicts of interest

The authors declare no conflicts of interest.

ORCID iDs

Alice Lunghi https://orcid.org/0000-0002-0191-8724
Matteo Genitoni https://orcid.org/0000-0002-4979-4302
Maria Letizia Focarete https://orcid.org/0000-0002-0458-7836
Michele Bianchi https://orcid.org/0000-0002-9660-9894

References

[1] Van Den Berg M E L, Castellote J M, Mahillo-Fernandez I and De Pedro-Cuesta J 2010 Incidence of spinal cord injury worldwide: a systematic review *Neuroepidemiology* **34** 184–92
[2] Ding W, Hu S, Wang P, Kang H, Peng R, Dong Y and Li F 2022 Spinal cord injury: the global incidence, prevalence, and disability from the global burden of disease study *Spine* **47** 1532–40
[3] Karsy M and Hawryluk G 2019 Modern medical management of spinal cord injury *Curr. Neurol. Neurosci. Rep.* **19** 65
[4] Courtine G and Sofroniew M V 2019 Spinal cord repair: advances in biology and technology *Nat. Med.* **25** 898–908
[5] Lorach H *et al* 2023 Walking naturally after spinal cord injury using a brain–spine interface *Nature* **618** 126–33
[6] Yamazaki K, Kawabori M, Seki T and Houkin K 2020 Clinical trials of stem cell treatment for spinal cord injury *Int. J. Mech. Sci.* **21** 3994
[7] Papa S, Pizzetti F, Perale G, Veglianese P and Rossi F 2020 Regenerative medicine for spinal cord injury: focus on stem cells and biomaterials *Expert Opin. Biol. Ther.* **20** 1203–13
[8] Schmidt C E and Leach J B 2003 Neural tissue engineering: strategies for repair and regeneration *Annu. Rev. Biomed. Eng.* **5** 293–347
[9] Boni R, Ali A, Shavandi A and Clarkson A N 2018 Current and novel polymeric biomaterials for neural tissue engineering *J. Biomed. Sci.* **25** 90
[10] Farhat W, Hasan A, Lucia L, Becquart F, Ayoub A and Kobeissy F 2019 Hydrogels for advanced stem cell therapies: a biomimetic materials approach for enhancing natural tissue function *IEEE Rev. Biomed. Eng.* **12** 333–51
[11] Mazzoni E, Iaquinta M R, Lanzillotti C, Mazziotta C, Maritati M, Montesi M, Sprio S, Tampieri A, Tognon M and Martini F 2021 Bioactive materials for soft tissue repair *Front. Bioeng. Biotechnol.* **9** 613787
[12] Wang Y *et al* 2022 Gene delivery of chitosan-graft-polyethyleneimine vectors loaded on scaffolds for nerve regeneration *Carbohydr. Polym.* **290** 119499
[13] Bianchi M, Guzzo S, Lunghi A, Greco P, Pisciotta A, Murgia M, Carnevale G, Fadiga L and Biscarini F 2023 Synergy of nanotopography and electrical conductivity of PEDOT/PSS for enhanced neuronal development *ACS Appl. Mater. Interfaces* **15** 59224–35
[14] Sun X *et al* 2019 Devising micro/nano-architectures in multi-channel nerve conduits towards a pro-regenerative matrix for the repair of spinal cord injury *Acta Biomater.* **86** 194–206
[15] De Ruiter G C W, Malessy M J A, Yaszemski M J, Windebank A J and Spinner R J 2009 Designing ideal conduits for peripheral nerve repair *Neurosurg. focus* **26** E5
[16] Chiono V and Tonda-Turo C 2015 Trends in the design of nerve guidance channels in peripheral nerve tissue engineering *Prog. Neurobiol.* **131** 87–104
[17] Kusuhara H, Hirase Y, Isogai N and Sueyoshi Y 2019 A clinical multi-center registry study on digital nerve repair using a biodegradable nerve conduit of PGA with external and internal collagen scaffolding *Microsurgery* **39** 395–9
[18] Czeisler C *et al* 2016 Surface topography during neural stem cell differentiation regulates cell migration and cell morphology *J. Comp. Neurol.* **524** 3485–502
[19] Iandolo D, Sheard J, Levy G K, Pitsalidis C, Tan E, Dennis A, Kim J-S, Markaki A E, Widera D and Owens R M 2020 Biomimetic and electroactive 3D scaffolds for human neural crest-derived stem cell expansion and osteogenic differentiation *MRS Commun.* **10** 179–87
[20] Lunghi A *et al* 2022 Flexible neural interfaces based on 3D PEDOT:PSS micropillar arrays *Adv. Mater. Interfaces* **9** 2200709
[21] Béduer A, Vieu C, Arnauduc F, Sol J-C, Loubinoux I and Vaysse L 2012 Engineering of adult human neural stem cells differentiation through surface micropatterning *Biomaterials* **33** 504–14
[22] Valle F, Chelli B, Bianchi M, Greco P, Bystrenova E, Tonazzini I and Biscarini F 2010 Stable non-covalent large area patterning of inert teflon-AF surface: a new approach to multiscale cell guidance *Adv. Eng. Mater.* **12** B185–91
[23] ElMahmoudy M, Curto V F, Ferro M, Hama A, Malliaras G G, O'Connor R P and Sanaur S 2019 Electrically controlled cellular migration on a periodically micropatterned PEDOT:PSS conducting polym. platform *J. Appl. Polym. Sci.* **136** 47029
[24] White R and Barry D 2015 The emerging roles of transplanted radial glial cells in regenerating the central nervous system *Neural. Regen. Res.* **10** 1548
[25] Simitzi C, Ranella A and Stratakis E 2017 Controlling the morphology and outgrowth of nerve and neuroglial cells: the effect of surface topography *Acta Biomater.* **51** 21–52
[26] Marcus M, Baranes K, Park M, Choi I S, Kang K and Shefi O 2017 Interactions of neurons with physical environments *Adv. Healthcare Mater.* **6** 1700267

[27] Song M and Uhrich K E 2007 Optimal micropattern dimensions enhance neurite outgrowth rates, lengths, and orientations *Ann. Biomed. Eng.* **35** 1812–20

[28] Cheng W L and Lin C C K 2004 The effects of different electrical stimulation protocols on nerve regeneration through silicone conduits *J. Trauma* **56** 1241–6

[29] Sordini L, Garrudo F F F, Rodrigues C A V, Linhardt R J, Cabral J M S, Ferreira F C and Morgado J 2021 Effect of electrical stimulation conditions on neural stem cells differentiation on cross-linked PEDOT:PSS films *Front. Bioeng. Biotechnol.* **9** 591838

[30] Pires F, Ferreira Q, Rodrigues C A V, Morgado J and Ferreira F C 2015 Neural stem cell differentiation by electrical stimulation using a cross-linked PEDOT substrate: expanding the use of biocompatible conjugated conductive polymers for neural tissue engineering *Biochim. Biophys. Acta* **1850** 1158–68

[31] Green R A, Baek S, Poole-Warren L A and Martens P J 2010 Conducting polymer-hydrogels for medical electrode applications *Sci. Technol. Adv. Mater.* **11** 014107

[32] Simon D T, Gabrielsson E O, Tybrandt K and Berggren M 2016 Organic bioelectronics: bridging the signaling gap between biology and technology *Chem. Rev.* **116** 13009–41

[33] Paulsen B D, Tybrandt K, Stavrinidou E and Rivnay J 2020 Organic mixed ionic–electronic conductors *Nat. Mater.* **19** 13–26

[34] Bianchi M, Carli S, Di Lauro M, Prato M, Murgia M, Fadiga L and Biscarini F 2020 Scaling of capacitance of PEDOT:PSS: volume *vs.* area *J. Mater. Chem.* C **8** 11252–62

[35] Zan J, Qian G, Deng F, Zhang J, Zeng Z, Peng S and Shuai C 2022 Dilemma and breakthrough of biodegradable poly-l-lactic acid in bone tissue repair *J. Mater. Res. Technol.* **17** 2369–87

[36] Panda A K and Basu B 2021 Biomaterials-based bioengineering strategies for bioelectronic medicine *Mater. Sci. Eng. R* **146** 100630

[37] Ghane N, Khalili S, Nouri Khorasani S, Esmaeely Neisiany R, Das O and Ramakrishna S 2021 Regeneration of the peripheral nerve via multifunctional electrospun scaffolds *J. Biomed. Mater. Res.* **109** 437–52

[38] Song J, Gao H, Zhu G, Cao X, Shi X and Wang Y 2016 The construction of three-dimensional composite fibrous macrostructures with nanotextures for biomedical applications *Biofabrication* **8** 035009

[39] Tsai N, She J, Wu J, Chen P, Hsiao Y and Yu J 2019 Poly(3,4-ethylenedioxythiophene) polymer composite bioelectrodes with designed chemical and topographical cues to manipulate the behavior of PC12 neuronal cells *Adv. Mater. Interfaces* **6** 1801576

[40] Gingras J, Rioux R M, Cuvelier D, Geisse N A, Lichtman J W, Whitesides G M, Mahadevan L and Sanes J R 2009 Controlling the orientation and synaptic differentiation of myotubes with micropatterned substrates *Biophys. J.* **97** 2771–9

[41] Bakeine G J, Ban J, Grenci G, Pozzato A, Zilio S D, Prasciolu M, Businaro L, Tormen M and Ruaro M E 2009 Design, fabrication and evaluation of nanoscale surface topography as a tool in directing differentiation and organisation of embryonic stem-cell-derived neural precursors *Microelectron. Eng.* **86** 1435–8

[42] English A *et al* 2015 Substrate topography: a valuable in vitro tool, but a clinical red herring for in vivo tenogenesis *Acta Biomater.* **27** 3–12

[43] Cordewener F W, Bos R R M, Rozema F R and Houtman W A 1996 Poly(l-lactide) implants for repair of human orbital floor defects: clinical and magnetic resonance imaging evaluation of long-term results *J.Oral Maxillofac. Surg.* **54** 9–13

[44] Gentile P, Chiono V, Carmagnola I and Hatton P 2014 An overview of poly(lactic-co-glycolic) acid (PLGA)-based biomaterials for bone tissue engineering *Int. J. Mech. Sci.* **15** 3640–59

[45] Hu J, Sun X, Ma H, Xie C, Chen Y E and Ma P X 2010 Porous nanofibrous PLLA scaffolds for vascular tissue engineering *Biomaterials* **31** 7971–7

[46] Dai Y, Lu T, Shao M and Lyu F 2022 Recent advances in PLLA-based biomaterial scaffolds for neural tissue engineering: fabrication, modification, and applications *Front. Bioeng. Biotechnol.* **10** 1011783

[47] Kim K D, Lee K S, Coric D, Harrop J S, Theodore N and Toselli R M 2022 Acute implantation of a bioresorbable polymer scaffold in patients with complete thoracic spinal cord injury: 24-month follow-up from the inspire study *Neurosurgery* **90** 668–75

[48] Singh Y 2013 Electrical resistivity measurements: a review *Int. J. Mod. Phys. Conf. Ser.* **22** 745–56

[49] Schneider C A, Rasband W S and Eliceiri K W 2012 NIH image to imageJ: 25 years of image analysis *Nat. Methods* **9** 671–5

[50] Faisal A A and Laughlin S B 2007 Stochastic simulations on the reliability of action potential propagation in thin axons *PLoS Comput. Biol.* **3** e79

[51] Hallab N J, Bundy K J, O'Connor K, Clark R and Moses R L 1995 Cell adhesion to biomaterials: correlations between surface charge, surface roughness, adsorbed protein, and cell morphology *J. Long-Term Eff. Med. Implants* **5** 209–31

[52] Ventre M, Valle F, Bianchi M, Biscarini F and Netti P A 2012 Cell fluidics: producing cellular streams on micropatterned synthetic surfaces *Langmuir* **28** 714–21

[53] Boi M *et al* 2015 Tough and adhesive nanostructured calcium phosphate thin films deposited by the pulsed plasma deposition method *RSC Adv.* **5** 78561–71

[54] Fan Y W, Cui F Z, Hou S P, Xu Q Y, Chen L N and Lee I-S 2002 Culture of neural cells on silicon wafers with nano-scale surface topograph *J. Neurosci. Methods* **120** 17–23

[55] Carli S, Bianchi M, Di Lauro M, Prato M, Toma A, Leoncini M, De Salvo A, Murgia M, Fadiga L and Biscarini F 2022 Multifunctionally-doped PEDOT for organic electrochemical transistors *Front. Mater.* **9** 1063763

[56] Guzzo S, Carli S, Pavan B, Lunghi A, Murgia M and Bianchi M 2021 Evaluation of the in vitro biocompatibility of PEDOT:nafion coatings *Nanomaterials* **11** 2022

[57] Bianchi M, Gambardella A, Berni M, Panseri S, Montesi M, Lopomo N, Tampieri A, Marcacci M and Russo A 2016 Surface morphology, tribological properties and in vitro biocompatibility of nanostructured zirconia thin films *J. Mater. Sci., Mater. Med.* **27** 96

[58] Tian Y, Yan S, Song C, Wang C and Chen J 2022 Research on the influence of Micro-morphology on the hydrophobicity of material surface *Colloids Interface Sci. Commun.* **46** 100556

[59] Koutsouras D A, Gkoupidenis P, Stolz C, Subramanian V, Malliaras G G and Martin D C 2017 Impedance spectroscopy of spin-cast and electrochemically deposited PEDOT:PSS films on microfabricated electrodes with various areas *ChemElectroChem* **4** 2321–7

[60] Kim Y, Yoo S and Kim J-H 2022 Water-based highly stretchable PEDOT:PSS/nonionic WPU transparent electrode *Polymers* **14** 949

[61] Kim S, Kim S Y, Chung M H, Kim J and Kim J H 2015 A one-step roll-to-roll process of stable AgNW/PEDOT:PSS solution using imidazole as a mild base for highly conductive and transparent films: optimizations and mechanisms *J. Mater. Chem.* C **3** 5859–68

[62] Da Silva D, Kaduri M, Poley M, Adir O, Krinsky N, Shainsky-Roitman J and Schroeder A 2018

Biocompatibility, biodegradation and excretion of polylactic acid (PLA) in medical implants and theranostic systems *Chem. Eng. J.* **340** 9–14

[63] Hakkarainen M, Albertsson A-C and Karlsson S 1996 Weight losses and molecular weight changes correlated with the evolution of hydroxyacids in simulated in vivo degradation of homo- and copolymers of PLA and PGA *Polym. Degrad. Stab.* **52** 283–91

[64] Lu L, Garcia C A and Mikos A G 1999 In vitro degradation of thin poly(DL-lactic-co-glycolic acid) films *J, Biomed. Mater. Res.* **46** 236–44

[65] Wu L and Ding J 2004 In vitro degradation of three-dimensional porous poly(d,l-lactide-co-glycolide) scaffolds for tissue engineering *Biomaterials* **25** 5821–30

[66] Cam D and Marucci M 1997 Influence of residual monomers and metals on poly (l-lactide) thermal stability *Polymer* **38** 1879–84

[67] Dumitru A C, Espinosa F M, Garcia R, Foschi G, Tortorella S, Valle F, Dallavalle M, Zerbetto F and Biscarini F 2015 In situ nanomechanical characterization of the early stages of swelling and degradation of a biodegradable polymer *Nanoscale* **7** 5403–10